ROYAL SOCIETY OF CHEMISTRY

PAPER

Check for updates

Carbon dots, a powerful non-toxic support for bioimaging by fluorescence nanoscopy and eradication of bacteria by photothermia†

H. Belkahla,‡[a] R. Boudjemaa,‡[b] V. Caorsi,[b] D. Pineau,[a] A. Curcio,[c] J. S. Lomas, [iD][a] P. Decorse,[a] A. Chevillot-Biraud,[a] T. Azaïs,[d] C. Wilhelm,[c] H. Randriamahazaka*[a] and M. Hémadi [iD] *[a]

Carbon Dots (CDs) are innovative materials which have potential applications in many fields, including nanomedicine, energy and catalysis. Here CDs were produced by the alkali-assisted ultrasonic route and characterized by several techniques to determine their composition and properties. Fluorescence nanoscopy using single-molecule localization microscopy shows that they have very good photophysical properties and a remarkable blinking behaviour at 405 nm. Moreover, these CDs are a safe material, non-toxic towards different cell lines (cancer and non-cancer cells) even at very high concentration, reflecting an excellent biocompatibility. Photothermia, *i.e.* their heating capacity under laser irradiation, was evaluated at two wavelengths and at several power densities. The resulting temperature increment was high ($5 < \Delta T < 45$ °C) and appropriate for biomedical applications. Bioimaging and photothermia were then performed on *E. coli*, a Gram(−) bacterium, incubated with CDs. Remarkably, by photothermia at 680 nm (0.3, 1 and 1.9 W cm^{-2}) or 808 nm (1.9 W cm^{-2}), CDs are able to eradicate bacteria in their exponential and stationary phases. Images obtained by 3D super-resolution microscopy clearly show the different CD distributions in surviving bacteria after mild photothermal treatment. These results confirm that CDs are multifunctional materials with a wide range of biomedical applications.

1. Introduction

Carbon nanomaterials have many interesting applications in the field of nanomedicine. They are becoming essential materials due to their diverse forms with different physical, chemical, optical, electrochemical and electrical properties.[1] Recently, a new class of carbon nanoparticles, less than 10 nm in diameter, appeared accidently during the purification of carbon nanotubes.[2] These are now described as "Carbon Dots" (CDs) and have attracted considerable attention because of their excellent dispersibility,[3] high chemical stability and photostability,[4] excellent biocompatibility,[5] low toxicity[6] and low cost

of fabrication.[7] There are, therefore, myriad possibilities for these nanoparticles in different domains of application, such as chemical sensing,[8] photocatalysis,[9,10] electrocatalysis,[11] bioimaging,[12,13] drug delivery,[14,15] photodynamic therapy,[16,17] biosensors,[18,19] *etc.*

Moreover, there are several ways of synthesizing them. The two main approaches are classified as "top-down" and "bottom-up". The first one is based on physical or chemical techniques (laser ablation,[20] chemical oxidation,[21] confined combustion,[22] *etc.*) which break down larger graphitic materials into smaller particles. The "bottom-up" approach has received considerable attention and is now the most popular way of producing CDs. The molecular precursors (carbohydrates, urea, citrate, *etc.*) play a central role in the formation of CDs through chemical synthesis or carbonization. Depending of the nature of the precursors, several methods can be used: chemical or hydrothermal oxidation,[23] microwave pyrolysis[24] or ultrasonic treatment.[4,25–27]

The bottom-up approach was used in this work to produce CDs from a low-cost precursor (glucose) by alkali-assisted ultrasonic irradiation according to a known procedure.[4,28,29] By a facile one-step sonochemical route ultrafine, stable fluorescent CDs with a homogeneous size distribution in the nano-range were obtained.[4] The ultrasonic cavitation process in liquids induces the formation of gas bubbles that grow and

[a]*Interfaces, Traitements, Organisation et Dynamique des Systèmes, Université Paris Diderot, Sorbonne Paris Cité, CNRS-UMR 7086, 15 rue Jean-Antoine de Baïf, 75205 Paris Cedex 13, France. E-mail: hemadi@univ-paris-diderot.fr; hyacinthe.randria@univ-paris-diderot.fr*

[b]*Abbelight, 6 rue Jean Calvin, 75005 Paris, France*

[c]*Laboratoire Matières et Systèmes Complexes, Université Paris Diderot, Sorbonne Paris Cité, CNRS-UMR 7057, 10 rue Alice Domon et Léonie Duquet, 75205 Paris Cedex 13, France*

[d]*Laboratoire de Chimie de la Matière Condensée de Paris, Sorbonne Université, CNRS-UMR 7574, Collège de France, 4 place Jussieu, 75005 Paris, France*

† Electronic supplementary information (ESI) available. See DOI: 10.1039/c9na00140a

‡ Contributed equally to this work.

collapse, thus producing local 5500 °C hot spots and pressures of several thousand atmospheres.[30] These locally harsh conditions are responsible for the formation of CDs.

A cutting-edge technique, Single-Molecule Localization Microscopy (SMLM)[31] was here implemented to validate the feasibility of using CDs as a multitasking tool for both calibration and bioimaging. SMLM techniques require the stochastic photoswitching and the detection of single spatially and temporally separated fluorophores. To achieve this, most of the fluorophores are forced into a long-lasting non-fluorescent state, named "dark state", allowing only a subpopulation to emit fluorescence at a given time.[32] SMLM approaches strongly depend on the photophysical properties of the fluorophores and their environment. To date, such photoswitching properties mainly concern organic fluorophores (such as rhodamines, cyanines and oxazines), fluorescent proteins (PA-GFP, mEos2, *etc.*) and reversibly-binding probes (Nile Red).

Recently, CDs have been reported as photoswitchable fluorescent probes,[33] making them applicable for nanoscopy and more especially for SMLM. Nevertheless, their use in the field of nanoscopy is relatively new and the photoswitching mechanism is still not yet properly understood.[33] Further research and development on the use of CDs as probes for nanoscopy is required. Here we demonstrate that CDs can be exploited in SMLM for both calibrating the system properties (*e.g.* the localization precision) and for nanostructural analysis by bioimaging.

Photothermal therapy (PTT) is based on the use of near-infrared (NIR) light-absorbing agents that convert laser energy into heat, causing irreversible cellular damage and destruction of malignant cells or bacteria. Recently, CDs were used as an agent for photothermia[34–36] to destroy cancer cells. Geng *et al.*[37] reported high photothermal conversion efficiency for nitrogen and oxygen co-doped CDs under 808 nm laser irradiation. Bao *et al.*[38] developed sulfur and nitrogen co-doped CDs with high conversion efficiency in mouse models under 655 nm laser irradiation. A very limited number of studies[39] have explored the photothermal properties of CDs to eradicate bacteria: the bactericidal effect of CDs on *Staphylococcus aureus* is enhanced by 808 nm laser irradiation.

The aim of the present study is to explore possible applications of CDs in nanomedicine. The CDs were first characterized by a large panel of techniques: dynamic light scattering (DLS), Fourier transform infrared spectroscopy (FTIR), transmission electron microscopy (TEM), UV-visible-NIR spectroscopy, MAS NMR spectroscopy and X-ray photoelectron spectroscopy (XPS) to define their composition. Fluorescence emission spectrophotometry was performed to evaluate their photoluminescence properties.

Escherichia coli (*E. coli*) was chosen as a model for the two nanomedicine applications: nanoscopy and photothermia. Nanoscopy was used for the bioimaging of *E. coli* incubated with CDs and to demonstrate their spontaneous blinking. Their photothermal properties, namely their heating ability and the effect of the temperature increment on the viability of *E. coli in vitro* in two growth phases (exponential and stationary) were finally investigated.

2. Results and discussion

2.1 Synthesis and spectrophotometric study

CDs were prepared from glucose as precursor in alkali medium under ultrasonic treatment. The conditions were different from the reported protocol[4] in that the power was increased; a dark brown suspension was obtained (Fig. SI-1†). The absorption spectrum (Fig. 1a) shows a shoulder at 360 nm, a band at 270 nm and non-negligible absorption in the visible and NIR (400–800 nm). The absorption peak at 270 nm is due mainly to the $\pi \rightarrow \pi^*$ and $n \rightarrow \pi^*$ transitions of C=C and C=O bonds, respectively. When a very dilute suspension of CDs (colourless) is irradiated with an UV lamp, the suspension is cyan-coloured (Fig. 1a). When the suspension is excited at 365 nm, two fluorescence emission peaks are observed at 450 and 500 nm. In Fig. 1b are recorded different photoluminescence (PL) spectra obtained upon excitation at progressively higher wavelengths from 270 nm to 620 nm. The brightness and the emission
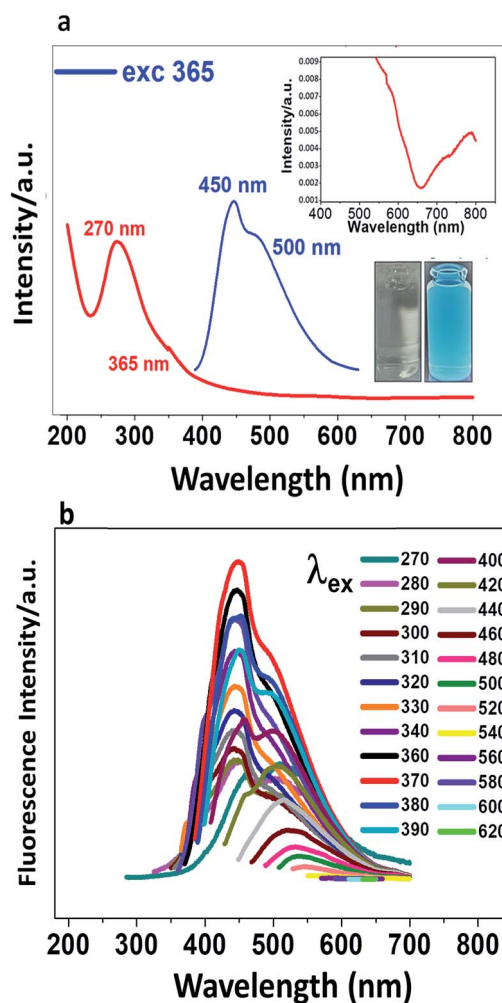

Fig. 1 (a) UV-visible absorption spectra (red), emission spectrum excited at 365 nm (blue) of a suspension of CDs. Insets: CD suspension under daylight (left) and 365 nm UV irradiation; (b) PL emission spectra of CDs at 10 ng ml^{-1} recorded for excitation at progressively higher wavelengths from 270 to 620 nm.

maximum vary with the excitation wavelength, the maximum shifting from shorter to longer wavelength as the excitation wavelength is increased.

To achieve the best fluorescence response of the CDs, their concentration and pH were optimized. Emission spectra were recorded at different pHs from 2 to 11. Fig. SI-2† shows that the maximum brightness is achieved at pH 8. At low pH, CDs are weakly charged and probably aggregated. Raising the pH increases the negative charge and reduces the aggregation, leading to an enhancement of the fluorescence intensity which maximises at pH 8, selected as the working pH for the rest of the study.

2.2 Structure and characterization

The morphology and the size of CDs were examined by transmission electron microscopy (TEM). Fig. 2 shows that the CDs are spherical and well dispersed. The histogram analysis of the TEM images gives an average diameter of approximately 2.5 nm (Fig. 2a and b). The average hydrodynamic size and distribution of the CDs were also evaluated by DLS (Fig. 2d), showing a narrow size range from 1 nm to 3 nm, which is consistent with the TEM results. These studies concur in that the CDs are roughly monodispersed spherical particles with a diameter between 2 and 3 nm. Their zeta potential in aqueous media at pH 8 is negative ($\xi = (-20 \pm 1)$ mV, Fig. 2c), due to the presence of hydroxyl, carbonyl and carboxyl groups on the surface.

The surface groups and the composition of CDs were identified by X-ray Photoelectron Spectroscopy (XPS) and compared to the spectra of glucose (Fig. 3). Relative elemental analysis for CDs shows: C: 63.2%; N: 0.13%; Na: 6.7% and O: 30.0%, hydrogen not being XPS-detectable. The measured C 1s XPS spectrum is deconvoluted into 3 peaks centred at 284.8 eV (non-oxygenated sp^3 C and sp^2 C, i.e. C–C and C=C), 286 eV (C–O), and 288 eV (C–C=O). The O 1s spectrum is dominated by two peaks at 531 and 532.5 eV due to C=O and C–O–H, respectively
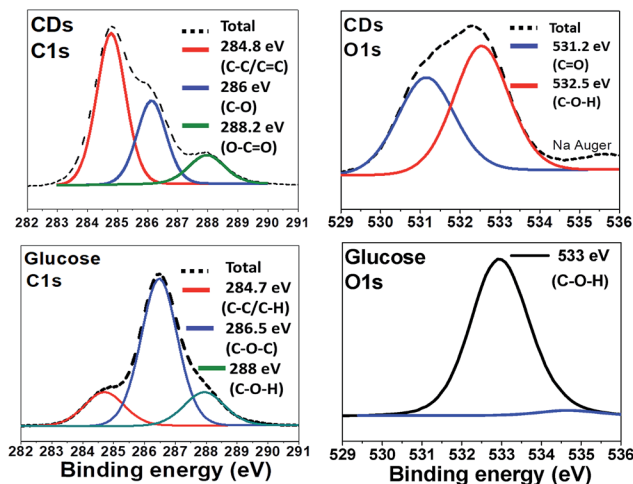

Fig. 3 High-resolution XPS spectra of C 1s and O 1s of CDs and glucose.

whereas for glucose only one peak, corresponding to C–O–H, appears at 533 eV.

To confirm this result, the CDs were examined by infrared spectroscopy (FTIR). In Fig. 4, the FTIR spectrum of CDs (Fig. 4a) is compared to that of glucose (Fig. 4b). The glucose spectrum (Fig. 4b) shows three main bands: a strong band at 3324 cm^{-1} for the hydroxyl groups and two smaller ones at 1645 and 750 cm^{-1} for C–O and C–H stretching, respectively.

The IR spectrum of the CDs (Fig. 4a) suggests the presence of abundant oxygen-containing functional groups formed during the carbonization process: broad band for hydroxyl O–H at 3331 cm^{-1}; COO$^-$ stretching vibrations at 1415 cm^{-1}; asymmetric and symmetric stretching of C–O–C in carboxylate groups at about 1350 cm^{-1} and 1080 cm^{-1}; C–H stretching vibrations of sp^3 carbon at 2920 and 2850 cm^{-1}; C=O stretching at around 1600 cm^{-1}.

The solid-state ^{13}C MAS NMR spectrum of the particles was assigned according to Cai et al.[40] and Baccile et al.,[41] and is in full agreement with the IR spectra, showing well defined bands for C–H, C–O–C, C–OH, O–C–O and C=O type carbons, with only a weak resonance for C=C carbon (Fig. 5). The resonances are consistent with the presence of carboxylate groups, ether and alcohol functions as well as aliphatic carbons.
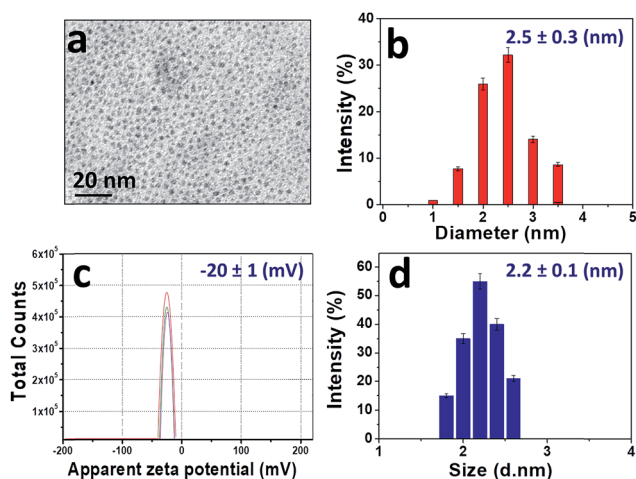

Fig. 2 (a) TEM image; (b) size histogram; (c) zeta potential at pH 8. Each line represents individual measurements of the same sample, which were used to obtain an average value; (d) DLS profile.
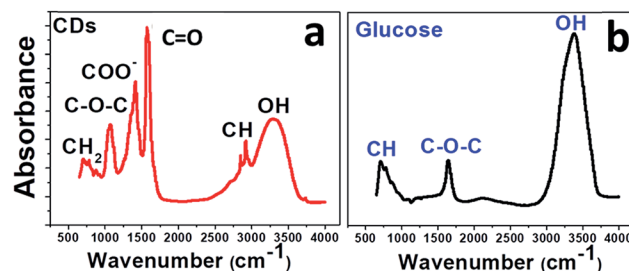

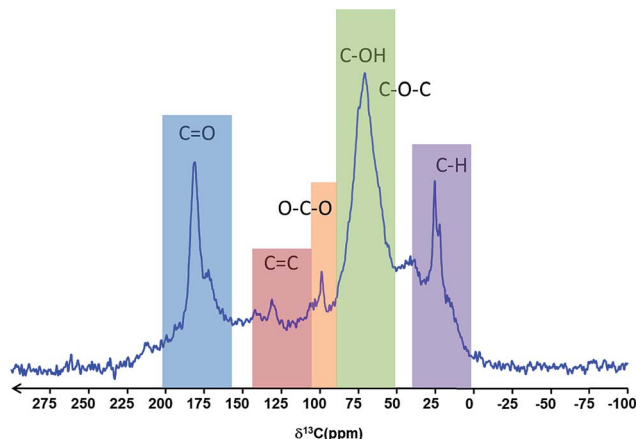Fig. 4 (a) FTIR spectra of the CDs and (b) glucose measured from 500 to 4000 cm^{-1}.

Fig. 5 ^{13}C MAS NMR spectrum of CDs.

Fig. 6 Heating curves of CDs (40 μg mL^{-1}) in PT mode under 808 and 680 nm laser (power: 0.3, 1, and 1.9 W cm^{-2}).

From the elemental analysis, the XPS, FTIR and NMR spectra, we infer the existence of oxygen-rich functional groups, such as carboxyl and hydroxyl, consistent with the high hydrophilicity and stability in aqueous media of the CDs.

Oxygen-containing functional groups are located at the surface of the CDs, and the corresponding surface states may induce intra-gap states between the π band (valence band) and the π* band (conduction band). The excitation wavelength-dependent photoluminescence (see above) is attributed to the surface groups which have various energy levels, resulting in a series of emissive traps.

2.3 Photothermia

The spectrophotometric study has highlighted the optical and photoluminescence properties of the CDs. The heat-producing ability under illumination with laser radiation (photothermia) was investigated. The surface-confined charges of the CDs are expected to contribute to the optical properties in the first biological visible/NIR window from 680 nm to 980 nm.[42]

Notably, their absorption at these wavelengths should be attributed to electron transitions between the trap-state energy levels on the surface. These trap-states play a major role in generating phonons (heat) through Shockley-Read-Hall electron–hole recombination or other defect-related paths.[35]

A fixed concentration of CDs (40 μg mL^{-1}) at pH 8, was irradiated at two different wavelengths (680 nm and 808 nm). Different laser power densities were investigated for each wavelength: 0.3, 1 and 1.9 W cm^{-2}. In Fig. 6, each sample was thermostated at 37 °C and after switching on the laser, the rise in temperature was plotted as a function of time. A plateau was reached after 8 minutes, whereupon the laser was switched off and the decrease in temperature was registered for a further 8 minutes. The highest temperature increments, 30 and 40 °C, were observed for 680 nm at 1 and 1.9 W cm^{-2}, respectively. Smaller increments were obtained for 808 nm at 1.9 W cm^{-2} (16 °C), for 680 nm at 0.3 W cm^{-2} (10 °C) and 808 nm at 1 W cm^{-2} (10 °C). Irradiation at 808 nm and 0.3 W cm^{-2} gave the lowest increase (3 °C). The heating can therefore be easily tuned through the laser power density and wavelength to attain the
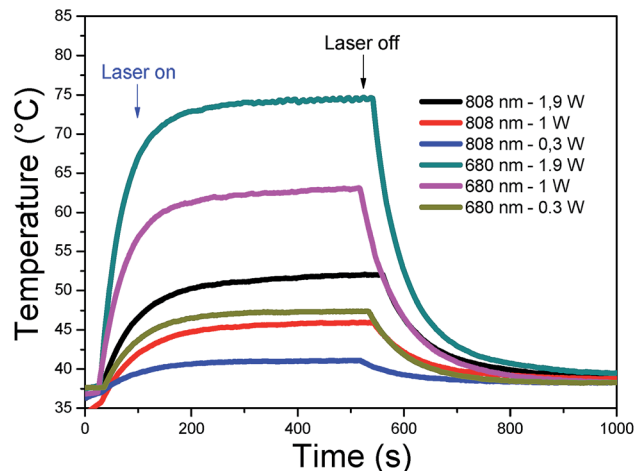
temperature range required for therapeutic applications at low CD concentrations. Overall, the excellent heating capacities of CDs make them good candidates for photothermal therapy.

2.4 Cytotoxicity

To check whether the use of CDs is favourable for medical applications, cytotoxicity was tested in two different cell lines: cancerous (Prostate cancer cells, PC-3) and non-malignant cells (Madin Darby Canine Kidney, MDCK.2). Methylene blue assay was used to perform the viability test at different CD concentrations from 0 to 500 μg mL^{-1}. PC-3 cells show a small decrease in viability (5%) starting at very high concentration (400 and 500 μg mL^{-1}) (Fig. 7). There is no significant loss in viability of MDCK.2 cells even at higher concentration. This result is consistent with the potential use of CDs to treat different pathologies such as cancer or bacterial infection.

2.5. Applications: multifunctionality of CDs

2.5.1 A single tool for calibration and bioimaging. Super-resolution microscopy or nanoscopy techniques comprise fluorescence microscopy with resolutions that are not limited by the diffraction of light.[43] Among them, SMLM is the only light microscopy technique that enables the imaging of individual

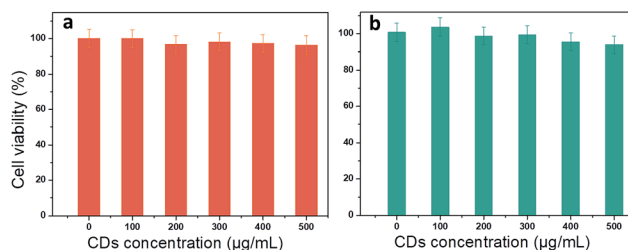Fig. 7 Methylene blue assay for cell viability after incubation with CDs at different concentrations (0−500 μg mL^{-1}) for 24 h of (a) cancer cells (PC-3); (b) non-malignant cells (MDCK.2). Error bars indicate the mean standard deviations ($n = 3$).

fluorescent molecules, achieving nanoscale precision (down to 15 nm). Recently, Bourg *et al.*[44] proposed a novel technology based on the detection of super-critical angle fluorescence, making it possible to retrieve 3D isotropic localization of individual molecules. In most cases, lateral and axial detection with such a precision requires a robust and accurate calibration to validate the experimental measures obtained with the instrument. Here, we propose CDs as a powerful non-toxic tool for enabling both calibration and bioimaging. To date, calibration has been performed using either photoswitching fluorescent molecules deposited on a coverslip (such as AF647 (ref. 45)) or fluorescent microspheres, of well-known diameter (generally 40 nm to 15 μm) loaded or coated with fluorophores.[31] However, the fluorescent molecules used in the first case tend to quickly photobleach, while in the second case the microsphere dimension is high, and the number of fluorophores is not accurately controlled. Using CDs, continuous imaging over a period of 5 minutes showed that the number of photons emitted under low laser irradiation (wavelength 639 nm, 40 mW) was constant (with an average of 1.2 K photons per detection over 50 ms of the camera integration time), indicating very good brightness accompanied by negligible photobleaching (Fig. 8a). Similar measurements performed on the commonly-used AF647 show lower brightness (760 photons per detection) and rapid photobleaching.[45]
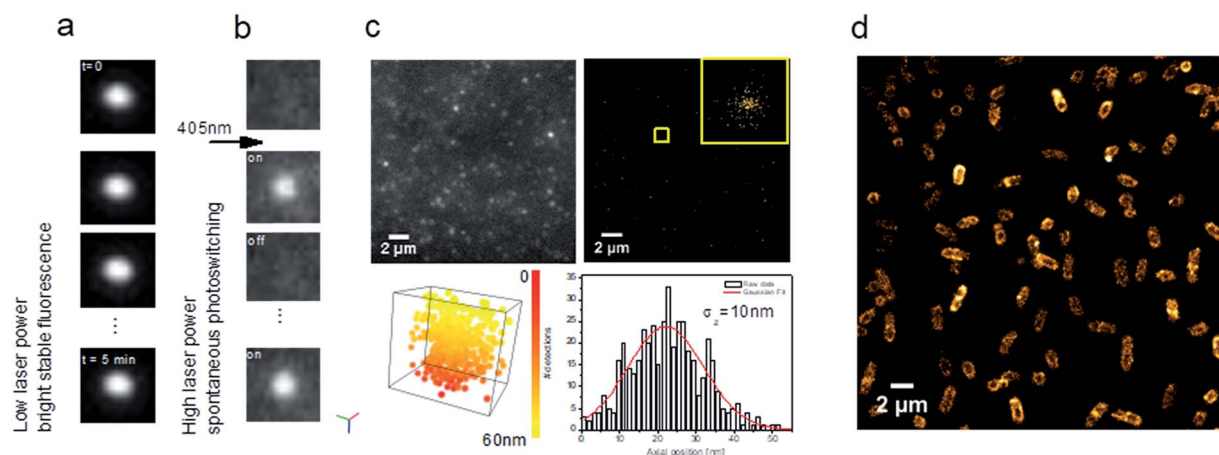
Interestingly, when the 639 nm laser power (as used in SMLM) is increased (200 mW) together with continuous 405 nm irradiation at low power, CDs exhibit spontaneous photoswitching (Fig. 8b; Video SI-1†). To the best of our knowledge, this intriguing phenomenon of reversible photoswitching has only been reported for photoswitchable fluorescent proteins[32] and very recently for the first time for CDs.[12,46] Excitation at 405 nm switches on CDs and 639 nm quenches them, while continuous excitation at 405 nm (1 mW) induces spontaneous

photoswitching of CDs. In contrast to commonly-used photoswitchable organic fluorophores, where blinking is induced by means of a specific imaging buffer (consisting usually of a thiol and oxygen-scavenging enzyme systems), the CDs spontaneously blink under continuous UV irradiation.

Given their photoswitching properties and their small size (2–10 nm), CDs are highly suitable for characterizing the performances of SMLM, in particular the localization precision σ (Fig. 8c), which to a first approximation is proportional to the standard deviation of the point spread function (the response of an imaging system to a point source) over N, the number of photons detected.[47] Fig. 8c shows the dispersion of localizations in 3D, indicating a localization precision of 10 nm for both the lateral and axial directions.

These photophysical properties make CDs particularly interesting fluorescent probes for SMLM and open up many applications in live-cell bioimaging, since in this case there is no need for specific imaging buffers which are, moreover, cytotoxic.[32,48] As a proof-of-concept for bioimaging, we used *E. coli* MG1655, a non-pathogenic Gram(−) bacterial strain. As shown in Fig. 8d, CDs were internalized and homogenously localized within the bacteria. A clustering analysis using the DBSCAN algorithm[49] led to an estimate of about 22 000 localizations per bacterium. These CDs can thus be used to obtain images of biological samples such as eukaryotic cells or bacteria, for example, with the same fluorophore used for calibration.

2.5.2 Photothermal treatment: the case of *E. coli*. *E. coli* contains a cell wall under a lipopolysaccharide layer. Certain strains of this bacterium are pathogenic and can cause urinary or gastrointestinal tract infections. A critical health problem[50] has arisen from the increasing resistance of *E. coli* to antibiotics. In general, bacteria can live in any environment as long as they have food as an energy source. Here, we investigate the

Fig. 8 Carbon dots as multi-tasking tools for single-molecule localization microscopy. (a) Representative images of a time series showing a stable bright fluorescence or (b) UV-induced blinking under continuous excitation at 639 nm; (c) TIRF image extracted from a time series (see ESI Video SI-1†) showing blinking of CD solution (left) and reconstructed image of *xy* localization (right). Inset shows *xy* dispersion for a single CD showing a standard deviation $\sigma_{x,y} = 10$ nm (bottom, left, Video SI-2†). 3D visualization of xyz localization (box size: *x*, *y*, *z* = 55 nm) (bottom, right). Axial localization distribution for a single CD. σ_z represents the standard deviation of the axial distribution. Colour bar corresponds to the axial position from 0 to 55 nm; (d) fluorescence nanoscopy image of *E. coli* incubated with CDs.

ability of CDs to eradicate *E. coli* by photothermia and how it depends on the bacterial growth phase, either exponential (when bacteria are actively dividing) or stationary (when the number of new cells produced balances the number of cells that die). This latter is characterized by significant physiological changes (such as membrane rigidification, slower metabolism) that occur due to nutrient loss. These physiological changes make bacteria in the stationary phase more resistant to external aggressions (antibiotics, nanoparticles, *etc.*[51]). In particular, *E. coli* has been shown to exhibit heat resistance when in the stationary phase.[52]

Exponentially-growing and stationary phase *E. coli* were incubated with CDs for 30 minutes at 37 °C and photothermal treatment was then performed by irradiating the sample for 8 minutes with a laser (680 nm or 808 nm). The temperature increment induced by irradiation of the CDs was then determined in each case and related to the survival rate (log N) of the bacteria (Fig. SI†). A bactericidal effect was defined as a 3-log reduction in bacterial counts compared to the control (without CDs). Fig. 9a shows that the exponential phase is sensitive to the temperature increment (Fig. SI-3,† $12 < \Delta T < 45$ °C) resulting from the irradiation with a 680 nm laser: while the effect was bactericidal at 0.3 or 1 W cm^{-2}, complete eradication was only found at 1.9 W cm^{-2}. Irradiation at 808 nm was ineffective at lower powers but led to a complete eradication at 1.9 W cm^{-2}. Against stationary phase cells, irradiation at 680 nm was ineffective at 0.3 W cm^{-2} and bactericidal at 1 W cm^{-2}. Complete eradication was achieved with both wavelengths at 1.9 W cm^{-2}. Consistently with previous literature data,[52] bacteria are more resistant to local heat increase in the stationary phase than in the exponential phase. The temperature increment induced by the CDs strongly correlates with bacterial killing. When the laser was applied to *E. coli* in the absence of CDs, bacteria continued to grow without any toxicity or alteration of log N in both growth phases (Fig. 9b). This shows that laser irradiation alone has no impact on bacterial development even at high power densities.
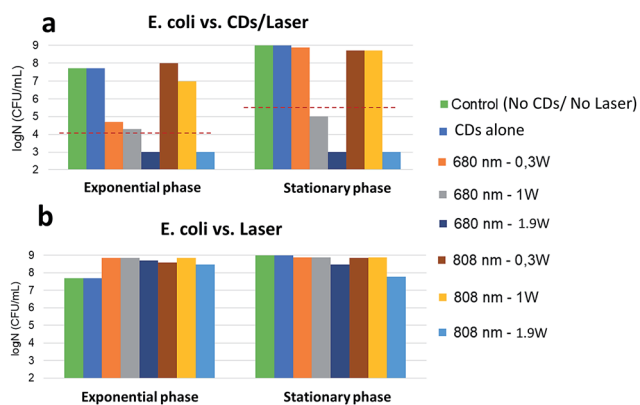
Using 3D nanoscopy before photothermal treatment, we show that the CDs are mainly internalized inside bacteria without any toxicity or damage (Fig. 10a, before photothermia). When *E. coli* were incubated with CDs, there are two possible situations after photothermal treatment: (i) complete eradication, and (ii) bactericidal effect with a subpopulation of surviving bacteria. In the case of complete eradication (log N < 3), no bacteria were visible under the microscope (figure not shown). In the intermediate case (Fig. 10a, after photothermia), CDs are preferentially localized at the bacterial poles and at the septum. The number of CD localizations per bacterium, assessed by the DBSCAN algorithm, is about 9000 at the poles and about 700 at the septum. This change in CD localization within bacteria could be explained by the fact that the poles of rod-shaped bacterial cells play an important role in various molecular processes, including DNA segregation, metabolic regulation and aggregate clearance.[53]

3. Experimental section

3.1 Synthetic procedures

CDs were synthesized directly from D-(β)-glucose by a one-step alkali-assisted ultrasonic treatment adapted from a reported method.[4] Briefly, a 1 M solution of D-(β)-glucose was prepared in a 0.5 M aqueous solution of NaOH. The mixture was then ultrasonicated for 4 hours (frequency 35 kHz, power 100% (750 W)) using an Elma TI-H-15 sonicator. The resulting CDs were obtained as a very stable and highly dispersed colloidal suspension,

Fig. 9 CFUs/mL of *E. coli* either in the stationary or the exponential growth phase, after laser irradiation (a) with or (b) without CDs, at two laser wavelengths (680 or 808 nm) and different powers (0.3, 1 or 1.9 W cm^{-2}).
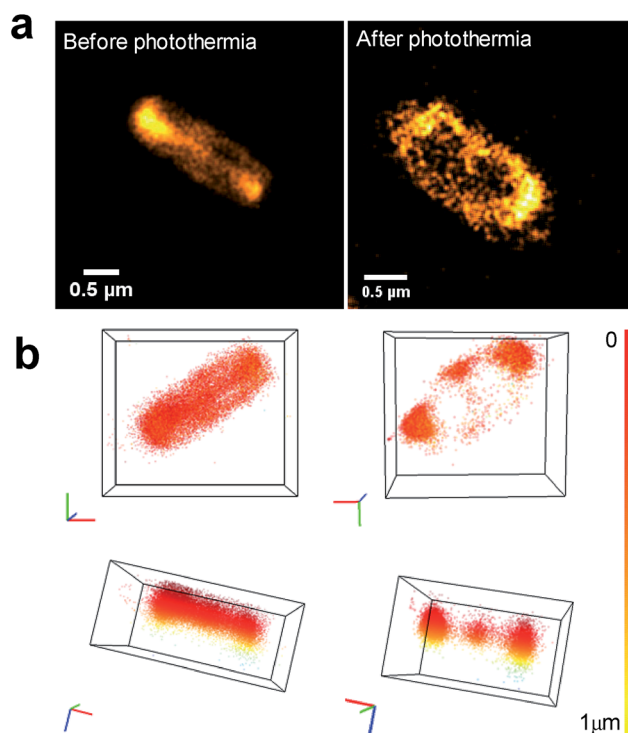

Fig. 10 (a) 2D nanoscopy images of bacteria before and after photothermia in the presence of CDs; (b) 3D visualization of carbon dots in bacteria (same as shown in (a)).

dark brown in our case and yellow according to the previous report (Fig. SI†). Excess glucose was removed in 24 h by means of a Float-A-Lyzer G2 dialysis device (MWCO 0.5–1 kDa). Finally the dark brown suspension of CDs was stored in the dark at 4 °C.

3.2 Materials and methods

3.2.1 Spectrophotometric measurements.
Absorption measurements were performed at 37 ± 0.5 °C on a Cary 4000 spectrophotometer equipped with Pelletier-thermostated cell-carriers. Fluorimetric measurements were performed at 37 ± 0.5 °C on a Fluorolog 3, Horiba Jobin Yvon spectrophotometer equipped with a thermostated cell-carrier. Emission spectra were measured in the 300–700 nm range for different excitation wavelengths (λ_{ex}) from 270 to 620 nm with an increment of 10 nm.

3.2.2 X-ray photoelectron spectroscopy (XPS).
The elemental composition and the bonding of the CDs were determined on a Thermo VG Scientific ESCALAB 250 equipped with a monochromatic Al Kα X-ray source at 1486.6 eV; spot size: 650 μm.

3.2.3 Fourier-transform infrared spectroscopy (FTIR).
FTIR transmission spectra were acquired on a Nicolet Magna-IR 860 spectrophotometer in the range 400–4000 cm^{-1}.

3.2.4 ^{13}C MAS NMR.
The NMR spectrum was recorded on a 700 Avance Bruker spectrometer operating at 16.4 Tesla. The corresponding Larmor frequency was 175 MHz. A 4 mm-diameter zirconia rotor was filled with lyophilized CD powder and then spun at the magic angle at 14 kHz. A 30° flip-angle pulse was used at a radio-frequency of 65 kHz. The recycle delay was 10 s. The ^{13}C chemical shifts were referenced to TMS (0 ppm).

3.2.5 Dynamic light scattering (DLS) and zeta potential.
The hydrodynamic diameter and the charge on the CDs were measured on Malvern Nano Zetasizer equipment at different pH values, using 10^{-2} M KNO$_3$ as the background electrolyte.

3.2.6 Transmission electron microscopy (TEM).
Transmission electron microscopy (TEM) was carried out to characterize sample morphology and size using a JEOL–100 CX microscope operating at 100 kV.

3.2.7 Cell toxicity.
Human prostate cancer (PC-3) cell line (ATCC® CRL-1435™) and Madin Darby Canine Kidney (MDCK.2) cell line (ATCC® CRL-2936™) were cultured in Dulbecco's modified Eagle's medium (DMEM) containing 10% fetal bovine serum, 1% penicillin, in a 5% CO$_2$ atmosphere at 37 °C. The cells (10^5 cells) were seeded into 24-well plates and allowed to adhere for 24 h. Then, a series of diluted CDs at different concentrations from (0 to 500 μg mL^{-1}) were added into the wells. After incubation for 24 h, the medium with the residual CDs was discarded and the cells were washed by PBS 3 times and fixed by methanol for 20 min at room temperature, washed three times in PBS and stained by 5% methylene blue for 30 min. After three subsequent gentle washes in PBS, methylene blue was eluted in 1% HCl for 4 h at ambient temperature. Optical density (OD) was then measured at 630 nm.

3.2.8 Bacterial strains and growth conditions.
The E. coli strain used in this study was "Escherichia coli MG1655". Previously stored at −80 °C in Luria Broth Miller (LB Miller, DIFCO, France) containing 20% (vol/vol) glycerol, the frozen cells were then subcultured twice in LB (one 8 h culture, followed by an overnight culture at 37 °C, 200 rpm). Working bacterial cultures were either in the stationary phase (harvested from an overnight culture) or in the exponential growth phase (obtained with a 1 : 100 subculture grown 3 h in LB).

3.2.9 Photothermal treatment.
Photothermia (PT) was induced by a continuous NIR laser at 680 nm or 808 nm (LASER Components S.A.S., France). The CD suspension (40 μg mL; volume = 50 μL), was used alone (as control) or incubated with bacteria at 37 °C for 30 minutes before irradiation. The sample was set at 37 °C by a home-made device and was illuminated for 8 minutes by a 1 cm^2 laser spot at different power densities: 0.3, 1 and 1.9 W cm^{-2}. The distance between the laser and the sample was 4 cm. The temperature elevation was recorded in real time with an infrared thermal-imaging camera (FLIR SC7000).

To assess the effect of the photothermal treatment on bacteria, each sample was centrifuged for 10 min at 5000g in order to eliminate the excess CD. The bacterial pellet was dispersed in 40 μL sterile NaCl (150 mM), centrifuged again and dispersed under the same conditions. Successive 10-fold dilutions were then made. For each dilution, three drops (10 μL) were deposited on Luria Broth agar (LB agar) plates, and incubated at 37 °C for 24 h. Colony Forming Units (CFUs) were counted and averaged for each dilution at each time. The detection limit of viable culturable cells was 100 CFU mL^{-1}.

3.2.10 Fluorescence nanoscopy using single-molecule localization microscopy.
The use of carbon dots for super-resolution microscopy was tested either on CD solutions alone or on bacteria incubated with CDs. (i) 50 μL of CD solution was deposited on a coverslip and directly imaged to characterize photophysical properties and blinking behaviour. (ii) Bacterial suspensions incubated with CDs with and without irradiation were fixed in 1% paraformaldehyde (Sigma) for 5 min at room temperature. Bacteria were then pelleted for 10 min at 5000g and twice washed with phosphate buffer.

3.2.11 Imaging and analysis.
All 2D and 3D images were taken using an inverted bright-field Olympus IX83 microscope equipped with a 100× oil-immersion objective with a high numerical aperture (1.49). To perform fluorescence nanoscopy experiments, a SAFe360 module (Abbelight, France) was added to the camera port of the microscope. This detection module couples Single-Molecule Localization Microscopy (SMLM), Supercritical Angle Fluorescence (SAF) and astigmatism[54] in a dual-view setup coupled with sCMOS cameras (Orcaflash v4, Hamamatsu). Prior to each acquisition, bright-light and diffraction-limited images were acquired. (i) Time lapse photos of CDs suspensions were taken at 2 Hz using continuous excitation at 639 nm in the TIRF mode; the fluorescence of bright spots was followed over a time period typical of biological STORM experiments, 20 000 frames. To induce blinking behaviour, irradiation at 405 nm was added at different time intervals. (ii) Bacteria were imaged by using continuous excitation at 639 nm, in the HiLo mode. Most of the fluorescent CDs were induced into a dark state until a sufficient density was

obtained (typically 1 molecule per bacterium per frame). Image series were recorded with a 50 ms exposure time. Resulting coordinate tables and images were processed and analyzed using SAFe NEO software (Abbelight, France).

4. Conclusions

CDs prepared from glucose by ultrasonic treatment open up many possibilities in several domains. We have established that they can be used as a tool for calibration and bioimaging, thanks to their remarkable photoluminescence and photoswitching properties. Photothermia by means of a laser at 680 nm produces enough heat to completely eradicate *E. coli* at relatively low power density. Further research could increase even further the absorption of CDs in the NIR region (800–1000 nm) by doping with heteroatoms in order to tailor them for applications in bioimaging and in the photothermal treatment of diseases, such as cancer or bacterial infection. Furthermore, functionalizing the surface of CDs, for instance, with proteins could enhance their targeting ability for these applications.

The exact molecular mechanism of photoswitching is still not fully understood. A better understanding of the structure–property correlation and the mechanism of blinking is the key to the development of applications of CDs in 3D fluorescence nanoscopy.

Conflicts of interest

There are no conflicts to declare.

Acknowledgements

Notes and references

1 Y. Zhang, M. Park, H. Y. Kim, B. Ding and S.-J. Park, *Sci. Rep.*, 2017, **7**, 45086.

2 X. Xu, R. Ray, Y. Gu, H. J. Ploehn, L. Gearheart, K. Raker and W. A. Scrivens, *J. Am. Chem. Soc.*, 2004, **126**, 12736–12737.

3 S. N. Baker and G. A. Baker, *Angew. Chem.*, 2010, **49**, 6726–6744.

4 H. Li, X. He, Y. Liu, H. Huang, S. Lian, S.-T. Lee and Z. Kang, *Carbon*, 2011, **49**, 605–609.

5 M. Havrdova, K. Hola, J. Skopalik, K. Tomankova, M. Petr, K. Cepe, K. Polakova, J. Tucek, A. B. Bourlinos and R. Zboril, *Carbon*, 2016, **99**, 238–248.

6 A. B. Bourlinos, A. Stassinopoulos, D. Anglos, R. Zboril, M. Karakassides and E. P. Giannelis, *Small*, 2008, **4**, 455–458.

7 H. L. Li, Z. Kang, Y. Liu and S. T. Lee, *J. Mater. Chem.*, 2012, **22**, 24230–24253.

8 D. Li, P. Jing, L. Sun, Y. An, X. Shan, X. Lu, D. Zhou, D. Han, D. Shen, Y. Zhai, S. Qu, R. Zboril and A. L. Rogach, *Adv. Mater.*, 2018, **30**, e1705913.

9 H. Yu, R. Shi, Y. Zhao, G. I. Waterhouse, L. Z. Wu, C. H. Tung and T. Zhang, *Adv. Mater.*, 2016, **28**, 9454–9477.

10 H. Li, X. He, Z. Kang, H. Huang, Y. Liu, J. Liu, S. Lian, C. H. Tsang, X. Yang and S. T. Lee, *Angew. Chem.*, 2010, **49**, 4430–4434.

11 C. Hu and L. Dai, *Angew. Chem.*, 2016, **55**, 11736–11758.

12 N. C. Verma, S. Khan and C. K. Nandi, *Methods Appl. Fluoresc.*, 2016, **4**, 044006.

13 L. Cao, X. Wang, M. J. Meziani, F. Lu, H. Wang, P. G. Luo, Y. Lin, B. A. Harruff, L. M. Veca, D. Murray, S. Y. Xie and Y. P. Sun, *J. Am. Chem. Soc.*, 2007, **129**, 11318–11319.

14 J. Tang, B. Kong, H. Wu, M. Xu, Y. Wang, Y. Wang, D. Zhao and G. Zheng, *Adv. Mater.*, 2013, **25**, 6569–6574.

15 Q. Wang, X. Huang, Y. Long, X. Wang, H. Zhang, R. Zhu, L. Liang, P. Teng and H. Zheng, *Carbon*, 2013, **59**, 192–199.

16 B. Tian, C. Wang, S. Zhang, L. Feng and Z. Liu, *ACS Nano*, 2011, **5**, 7000–7009.

17 X. Tu, Y. Ma, Y. Cao, J. Huang, M. Zhang and Z. Zhang, *J. Mater. Chem. B*, 2014, **2**, 2184–2192.

18 J. C. G. Esteves da Silva and H. M. R. Gonçalves, *TrAC, Trends Anal. Chem.*, 2011, **30**, 1327–1336.

19 X. Sun and Y. Lei, *TrAC, Trends Anal. Chem.*, 2017, **89**, 163–180.

20 J. Wang, C. F. Wang and S. Chen, *Angew. Chem.*, 2012, **51**, 9297–9301.

21 M. J. Krysmann, A. Kelarakis and E. P. Giannelis, *Green Chem.*, 2012, **14**, 3141–3145.

22 A. Rahy, Y. Zhou, J. Zheng, S. Y. Park, M. J. Kim, I. K. Jang, S. J. Cho and D. J. Yang, *Carbon*, 2012, **50**, 1298–1302.

23 A. A. P. Mansur, H. S. Mansur, F. P. Ramanery, L. C. Oliveira and P. P. Souza, *Appl. Catal., B*, 2014, **158–159**, 269–279.

24 T.-N. Pham-Truong, T. Petenzi, C. Ranjan, H. Randriamahazaka and J. Ghilane, *Carbon*, 2018, **130**, 544–552.

25 Z. Zhang, C. Fang, X. Bing and Y. Lei, *Materials*, 2018, **11**, 512.

26 X. Shan, L. Chai, J. Ma, Z. Qian, J. Chen and H. Feng, *Analyst*, 2014, **139**, 2322–2325.

27 Y. Liu, C. Y. Liu and Z. Y. Zhang, *J. Colloid Interface Sci.*, 2011, **356**, 416–421.

28 V. B. Kumar, Z. Porat and A. Gedanken, *Ultrason. Sonochem.*, 2016, **28**, 367–375.

29 H. Li, Z. Kang, Y. Liu and S.-T. Lee, *J. Mater. Chem.*, 2012, **22**, 24230.

30 J. J. Hinman and K. S. Suslick, *Top. Curr. Chem.*, 2017, **375**, 1–36.

31 C. Cabriel, N. Bourg, G. Dupuis and S. Leveque-Fort, *Opt. Lett.*, 2018, **43**, 174–177.

32 B. Turkowyd, D. Virant and U. Endesfelder, *Anal. Bioanal. Chem.*, 2016, **408**, 6885–6911.

33 S. Khan, N. C. Verma, A. Gupta and C. K. Nandi, *Sci. Rep.*, 2015, **5**, 11423.

34 M. Zheng, Y. Li, S. Liu, W. Wang, Z. Xie and X. Jing, *ACS Appl. Mater. Interfaces*, 2016, **8**, 23533–23541.

35 C. Lee, W. Kwon, S. Beack, D. Lee, Y. Park, H. Kim, S. K. Hahn, S. W. Rhee and C. Kim, *Theranostics*, 2016, **6**, 2196–2208.

36 M. Lan, S. Zhao, Z. Zhang, L. Yan, L. Guo, G. Niu, J. Zhang, J. Zhao, H. Zhang, P. Wang, G. Zhu, C.-S. Lee and W. Zhang, *Nano Res.*, 2017, **10**, 3113–3123.

37 B. Geng, D. Yang, D. Pan, L. Wang, F. Zheng, W. Shen, C. Zhang and X. Li, *Carbon*, 2018, **134**, 153–162.

38 X. Bao, Y. Yuan, J. Chen, B. Zhang, D. Li, D. Zhou, P. Jing, G. Xu, Y. Wang, K. Hola, D. Shen, C. Wu, L. Song, C. Liu, R. Zboril and S. Qu, *Light: Sci. Appl.*, 2018, **7**, 91.

39 N. Sattarahmady, M. Rezaie-Yazdi, G. H. Tondro and N. Akbari, *J. Photochem. Photobiol., B*, 2017, **166**, 323–332.

40 W. Cai, R. D. Piner, F. J. Stadermann, S. Park, M. A. Shaibat, Y. Ishii, D. Yang, A. Velamakanni, S. J. An, M. Stoller, J. An, D. Chen and R. S. Ruoff, *Science*, 2008, **321**, 1815–1817.

41 N. Baccile, G. Laurent, F. Babonneau, F. Fayon, M.-M. Titirici and M. Antonietti, *J. Phys. Chem. C*, 2009, **113**, 9644–9654.

42 D. Jaque, L. Martinez Maestro, B. del Rosal, P. Haro-Gonzalez, A. Benayas, J. L. Plaza, E. Martin Rodriguez and J. Garcia Sole, *Nanoscale*, 2014, **6**, 9494–9530.

43 L. Schermelleh, A. Ferrand, T. Huser, C. Eggeling, M. Sauer, O. Biehlmaier and G. P. C. Drummen, *Nat. Cell Biol.*, 2019, **21**, 72–84.

44 N. Bourg, C. Mayet, G. Dupuis, T. Barroca, P. Bon, S. Lécart, E. Fort and S. Lévêque-Fort, *Nat. Photonics*, 2015, **9**, 587–594.

45 G. T. Dempsey, M. Bates, W. E. Kowtoniuk, D. R. Liu, R. Y. Tsien and X. Zhuang, *J. Am. Chem. Soc.*, 2009, **131**, 18192–18193.

46 H. Wang, Y. Rivenson, Y. Jin, Z. Wei, R. Gao, H. Gunaydin, L. A. Bentolila, C. Kural and A. Ozcan, *Nat. Methods*, 2019, **16**, 103–110.

47 A. V. Diezmann, Y. Shechtman and W. E. Moerner, *Chem. Rev.*, 2017, **117**, 7244–7275.

48 A. G. Godin, B. Lounis and L. Cognet, *Biophys. J.*, 2014, **107**, 1777–1784.

49 M. Ester, H.-P. Kriegel, R. G. Sander and X. Xu, Presented in part at the *Proceedings of the Second International Conference on Knowledge Discovery and Data Mining*, Portland, Oregon, 1996.

50 S. T. Odonkor and K. K. Addo, *Int. J. Microbiol.*, 2018, **2018**, 7204013.

51 J. M. N. Llorens, A. Tormo and E. Martinez-Garcia, *FEMS Microbiol. Rev.*, 2010, **34**, 476–495.

52 D. S. Arora and J. Kaur, *Int. J. Antimicrob. Agents*, 1999, **12**, 257–262.

53 S. Govindarajan, N. Albocher, T. Szoke, A. Nussbaum-Shochat and O. Amster-Choder, *Front. Microbiol.*, 2017, **8**, 2695.

54 C. Cabriel, N. Bourg, P. Jouchet, G. Dupuis, C. Leterrier, A. Baron, M.-A. Badet-Denisot, B. Vauzeilles, E. Fort and S. Lévêque-Fort, *Nat. Commun.*, 2019, **10**, 1–10.